Mathematical Modelling and Analysis
Volume 15 Number 2, 2010, pages 199–222
Doi:10.3846/1392-6292.2010.15.199-222

ISSN 1392-6292 print
ISSN 1648-3510 online
www.vgtu.lt/mma/

A New Strategy for Choosing the Chebyshev-Gegenbauer Parameters in a Reconstruction Based on Asymptotic Analysis

Z. Jackiewicz[1,2] and **R. Park**[1]

[1] *School of Mathematics and Statistical Sciences, Arizona State University*
Tempe, AZ 85287, U.S.A.
[2] *AGH University of Science and Technology*
Kraków, Poland
E-mail(*corresp.*): jackiewi@math.la.asu.edu
E-mail: rpark@asu.edu

Received June 25, 2009; revised November 04, 2009; published online April 20, 2010

Abstract. The Gegenbauer reconstruction method, first proposed by Gottlieb et. al. in 1992, has been considered a useful technique for re-expanding finite series polynomial approximations while simultaneously avoiding Gibbs artifacts. Since its introduction many studies have analyzed the method's strengths and weaknesses as well as suggesting several applications. However, until recently no attempts were made to optimize the reconstruction parameters, whose careful selection can make the difference between spectral accuracies and divergent error bounds.

In this paper we propose asymptotic analysis as a method for locating the optimal Gegenbauer reconstruction parameters. Such parameters are useful to applications of this reconstruction method that either seek to bound the number of Gegenbauer expansion coefficients or to control compression ratios. We then illustrate the effectiveness of our approach with the results from some numerical experiments.

Keywords: Chebyshev pseudo-spectral approximation; Gegenbauer reconstruction; exponential convergence.

AMS Subject Classification: 42A25; 42A30; 65D10.

1 Introduction

Reconstruction methods are judged primarily by the rate at which their error approaches zero as the source resolution grows without bound. Since global reconstruction methods, in particular expansions of orthogonal polynomial basis functions, offer the possibility of exponential convergence, they are routinely chosen over local methods [12, 18]. The unfortunate reality is of course that such accuracy can be degraded whenever there exist discontinuities in the source

function we are trying to faithfully reconstruct. Indeed, the circumstances leading to so-called Gibbs artifacts are well understood and many strategies exist to minimize or, in some cases, eliminate them [8, 18, 22, 23].

One reconstruction strategy that addresses the Gibbs phenomenon is the Gegenbauer method described in [15, 16]. This method is based on a reprojection of the source data, e.g. Chebyshev or Fourier coefficients, onto a finite set of orthogonal Gegenbauer polynomials. This method then expands the new coefficients on sub-domains of physical space segmented by presumed jump discontinuities in the source data. The absence of jump discontinuities within each sub-domain assures spectral convergence as long as reconstruction parameters described in Section 2 are chosen carefully.

The explicit benefit of Gegenbauer method reconstruction to eliminate the Gibbs artifacts has been understood for nearly two decades. However, there are competing interests governing the selection of each reconstruction parameter. On one hand the choice of these parameters is limited to domains of numerical stability, but on the other hand we know that for analytical accuracy to increase, these same parameters must tend toward the very regions of instability we'd rather avoid. In fact, these numerical and analytical challenges have prompted the consideration of Freud polynomials as a significant improvement over Gegenbauer polynomials [11]. Freud polynomials are however not as well known and will take time before they are more commonly used. In the mean time, methods for optimizing Gegenbauer parameters, in particular those that could also be applied to newer polynomial basis sets, are needed.

Our last study demonstrated how asymptotic analysis could be used to find the Chebyshev-Gegenbauer reconstruction parameters best suited for avoiding numerical instability [20]. In this paper we again use asymptotic analysis as a method for locating optimal parameters for a Chebyshev-Gegenbauer reconstruction. Here however we have modified the constraint so that the optimal parameters will be useful to applications seeking to either bound the number of Gegenbauer expansion coefficients or to control compression ratios. Also, unlike the approach used in [20], which could only be determined numerically, here we will be able to predict the solutions analytically prior to demonstrating them numerically.

In Section 2 we provide a necessary backround and notation describing the Chebyshev-Gegenbauer reconstruction method. Then in Section 3 we analyze the behavior of error bounds for the truncation and regularization errors depending on different smoothness characteristics of the underlying function. In Section 4 we describe one-dimensional strategies for choosing the reconstruction parameter λ when given the resolution N and for choosing N when given λ. This section also provides sufficient insight into determining λ and N simultaneously for a two-dimensional minimization strategy. These techniques are then discussed in Section 5. Subsequently, in Section 6, we present the results of numerical experiments on both one and two-dimensional functions and thus illustrate the effectiveness of the strategies proposed in Section 5. Then in Section 7, we summarize the changes expected in the reconstruction error upper bounds when our sample data comes from either a Fourier–Galerkin or collocation expansion in contrast to the Gegenbauer, specifically Chebyshev,

expansion we used in the current and preceding sections. Finally, Section 8 provides concluding remarks and plans for future research.

2 Background and Notation

Consider the truncated Chebyshev pseudo-spectral expansion $f_N(x)$ of the real function $f(x)$, $f : [-1, 1] \to R$

$$f_N(x) = \sum_{n=0}^{N} a_n T_n(x), \tag{2.1}$$

where the coefficients a_n are computed from the formula

$$a_n = \frac{2}{N\tilde{c}_n} \sum_{j=0}^{N} \frac{1}{\tilde{c}_j} f(x_j) \cos\Big(\frac{\pi j n}{N}\Big), \quad n = 0, 1, \ldots, N.$$

Here, $\tilde{c}_0 = \tilde{c}_N = 2$, $\tilde{c}_n = 1$, $n = 1, 2, \ldots, N-1$, $T_n(x) = \cos\big(n \arccos(x)\big)$ are Chebyshev orthogonal polynomials defined on the interval $[-1, 1]$, and $x_j = \cos(\pi j/N)$, $j = 0, 1, \ldots, N$, are the Chebyshev-Gauss-Lobatto points.

If the function $f(x)$ is not analytic on the interval $[-1, 1]$ then $f_N(x)$ shows $O(1)$ spurious oscillations near the boundaries of $[a, b]$, the region of analyticity, and only $O(1/N)$ convergence within the same interval, the behavior known as the Gibbs phenomenon. So, consider this subinterval $[a, b] \subset [-1, 1]$ on which the function $f(x)$ is smooth, and denote by ξ the local variable defined by $x = x(\xi) = \epsilon\xi + \delta$, where $\epsilon = (b - a)/2$ and $\delta = (b + a)/2$ which maps the interval $[-1, 1]$ onto $[a, b]$. Within the context of this localization, Gottlieb *et al.* [13, 15, 16, 17] demonstrated that it is possible to overcome Gibbs behavior by re-expanding $f_N(x)$ in the Gegenbauer basis, i.e. orthogonal polynomials $C_l^\lambda(\xi)$ on the interval $[-1, 1]$ with the weight function $w(\xi) = (1 - \xi^2)^{\lambda - \frac{1}{2}}$ depending on the parameter λ. Here, l stands for the degree of $C_l^\lambda(\xi)$. We refer to [1, 7] for the definition and properties of these polynomials. The resulting truncated Gegenbauer series

$$f_g^{m,\lambda}(\epsilon\xi + \delta) = \sum_{l=0}^{m} \hat{g}_l^\lambda C_l^\lambda(\xi), \tag{2.2}$$

with the coefficients $\hat{g}_l^\lambda$ given by

$$\hat{g}_l^\lambda = \frac{1}{h_l^\lambda} \int_{-1}^{1} (1 - \xi^2)^{\lambda - \frac{1}{2}} f_N(\epsilon\xi + \delta) C_l^\lambda(\xi) d\xi \tag{2.3}$$

then provides an exponentially convergent approximation to the point values of the function $f(x)$ on the interval of smoothness $[a, b]$ including the boundaries a and b. Many edge detection techniques have been suggested as a means of identifying a and b, but they are not the focus of this current study. The novelty of computing Gegenbauer coefficients as shown in equation (2.3) is due first to the fact that $\hat{g}_l^\lambda$ can actually be computed since $f_N(x)$ is defined as

in (2.1) and the appropriate scaling factor, h_l^λ, is defined in [13]. Second, we recall from [17] that if λ and m are defined as

$$\lambda = \lceil \alpha \epsilon N \rceil, \quad m = \lceil \beta \epsilon N \rceil, \tag{2.4}$$

with carefully chosen constants α and β, the values of $\hat{g}_l^\lambda$ are exponentially accurate approximations of the exact Gegenbauer coefficients,

$$\hat{f}_l^\lambda = \frac{1}{h_l^\lambda} \int_{-1}^{1} (1-\xi^2)^{\lambda - \frac{1}{2}} f(\epsilon\xi + \delta) C_l^\lambda(\xi) d\xi, \tag{2.5}$$

as $N \to \infty$, and correspond to the exact truncated Gegenbauer series

$$f^{m,\lambda}(\epsilon\xi + \delta) = \sum_{l=0}^{m} \hat{f}_l^\lambda C_l^\lambda(\xi).$$

Denote by $\|f\|_\infty$ the supremum norm defined by $\|f\|_\infty := \sup_{x\in[a,b]} |f(x)|$ on the interval of smoothness. The total error $\|f - f_g^{m,\lambda}\|_\infty$ can be bounded by

$$\|f - f_g^{m,\lambda}\|_\infty \le \|f - f^{m,\lambda}\|_\infty + \|f^{m,\lambda} - f_g^{m,\lambda}\|_\infty.$$

The first term on the right hand side of the above inequality is the regularization error and the second is the truncation error. It was proved in [13, 15] that these errors can be bounded by

$$TE := \|f^{m,\lambda} - f_g^{m,\lambda}\|_\infty = \Big|\Big| \sum_{l=0}^{m} \Big(\hat{f}_l^\lambda - \hat{g}_l^\lambda\Big) C_l^\lambda \Big|\Big|_\infty \le A(N) q_T^{\epsilon N}, \tag{2.6}$$

$$RE := \|f - f^{m,\lambda}\|_\infty = \Big|\Big| f - \sum_{l=0}^{m} \hat{f}_l^\lambda C_l^\lambda \Big|\Big|_\infty \le \tilde{A}(N) q_R^{\epsilon N}, \tag{2.7}$$

where $A(N)$ and $\tilde{A}(N)$ grow at most as polynomials in N, and the ratios q_T and q_R are less than one for some range of the parameters α and β. The bounds (2.6) and (2.7) imply spectral convergence of $f_g^{m,\lambda}(x)$ to $f(x)$ as $N \to \infty$ on the interval $[a, b]$.

The ratio q_T corresponding to the truncation error TE takes the form

$$q_T = (\beta + 2\,\alpha)^{\beta + 2\,\alpha} / (2^\alpha \alpha^\alpha \beta^\beta), \tag{2.8}$$

as shown in [15]. The ratio q_R corresponding to the regularization error RE can be defined in different ways depending on the smoothness characteristics of the function $f(x)$. If there exists a constant $0 \le r_0 < 1$ and an analytic extension of $f(x)$ onto the elliptic domain

$$D_{\epsilon,\delta} = \Big\{ z : \; z = \frac{\epsilon}{2}\Big(r e^{i\theta} + \frac{1}{r} e^{-i\theta} \Big) + \delta, \quad 0 \le \theta \le 2\pi, \; r_0 \le r < 1 \Big\},$$

then the regularization ratio q_R is defined by

$$q_R = q_{R,1} = \frac{(\beta + 2\alpha)^{\frac{\beta + 2\alpha}{2}}}{(2\alpha)^\alpha \beta^{\frac{\beta}{2}}} (\epsilon r_0)^\beta, \tag{2.9}$$

as shown in [15]. These elliptic regions $D_{\epsilon,\delta}$ are displayed in Fig. 1 for $[a,b] = [-1,1]$ which corresponds to $\epsilon = 1$, $\delta = 0$, and for the parameter $r_0 = 0.1, 0.12, \ldots, 0.5$, where the largest ellipse corresponds to $r_0 = 0.1$ and the smallest to $r_0 = 0.5$. We have also displayed on this figure the interval $[-1,1]$ by the thick line. Alternatively, if there exist constants $\rho \geq 1$ and $C(\rho) \geq 0$

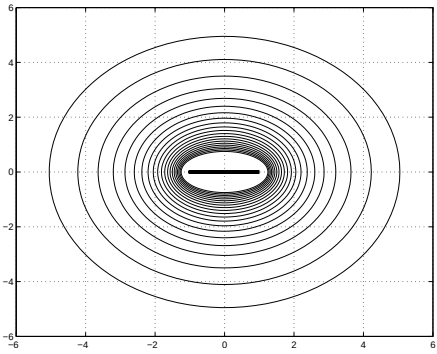

Figure 1. The elliptic regions $D_{1,0}$ for $r_0 = 0.1, 0.12, \ldots, 0.5$; the interval $[-1,1]$ is displayed by the thick line.

such that the kth derivative $f^{(k)}(x)$ can be bounded by

$$\|f^{(k)}\|_\infty \leq C(\rho)\frac{k!}{\rho^k}, \quad k \geq 0, \tag{2.10}$$

then the regularization ratio q_R is defined by

$$q_R = q_{R,2} = \frac{(\beta+2\alpha)^{\beta+2\alpha}\epsilon^\beta}{2^{\beta+2\alpha}\alpha^\alpha(\alpha+\beta)^{\alpha+\beta}\rho^\beta}, \tag{2.11}$$

as shown in [15]. Here, ρ is the distance from $[a,b]$ to the nearest singularity of $f(x)$ in the complex plane. The bound (2.7) may still be useful for $\rho < 1$ as long as $q_{R,2} < 1$. The relationship between r_0 and ρ is discussed in [10]. The parameters α and β appearing in (2.9) and (2.11) are defined by (2.5).

Clearly, the convergence rate of $f_g^{m,\lambda}(x)$ to $f(x)$ on the interval $[a,b]$ depends critically on the choice of α and β. A strategy for choosing optimal parameters α and β for given values of N was first investigated in [9]. A refinement of this strategy, where α and β were chosen independently of N, was then presented in [10] and [19]. In [10] we also described a strategy for the automatic determination of smoothness parameters r_0 and ρ.

Subsequent to choosing α and β as directed from any one of the strategies above, the parameters λ and m, subject to equation (2.4), tend to infinity as $N \to \infty$. There are however applications of Gegenbauer reconstruction which require that the parameter m be bounded, such as those cases where compression must be controlled or even maximized. In this paper we will demonstrate that for such circumstances the truncation error tends to zero as $N \to \infty$ while the regularization error simultaneously diverges to infinity

or converges to a constant different from zero as $N \to \infty$. As a result, the approaches taken in [9, 10, 19] for choosing α and β are no longer applicable and a different tact is required.

We will then describe how the results of an asymptotic analysis help to frame subsequent, and very revealing, one and two-dimensional optimization results. These results, realized via numerical minimization, identify optimal values of α and N for use in Gegenbauer reconstructions that require the number of terms, m, to be bounded or fixed. Granted, for a fixed m, the Gegenbauer reconstruction's error bound still diverges to infinity or tends to a nonzero constant as N grows without bound, it will nevertheless be shown to reach quite small minimal values for appropriately chosen α and N. As we shall see, such minimal values of error will likely be acceptable for many practical applications. Finally, we recognize that there are a significant number of symbols in this study and thus refer the reader to the symbol table in our last paper, [20].

3 Behavior of Error Bounds for the Gegenbauer Method in Applications to Compression

To simplify the presentation in this section we will write N, r_0 and ρ instead of ϵN, ϵr_0 and ρ/ϵ. Also, we will always assume that the number of terms m in the truncated Gegenbauer series (2.2) is fixed. As already mentioned in Section 2 such situations occur in the application of Gegenbauer reconstruction to compression. We consider first the behavior of q_T and q_T^N as $N \to \infty$. Substituting $\beta = m/N$ into q_T defined by (2.8) we obtain

$$q_T = q_T(\alpha, N, m) = \Big(1 + \frac{2\alpha N}{m}\Big)^{\frac{m}{N}} \Big(\frac{m}{N} + 2\alpha\Big)^{2\alpha} \big(2\alpha\big)^{-\alpha}. \tag{3.1}$$

For given N and m consider the one-dimensional minimization problem

$$q_T(\alpha, N, m) \to \min .$$

The solution $\alpha_{opt} = \alpha_{opt}(N, m)$ to this problem is plotted in Fig. 2 versus the number N. We have also plotted in the middle graph of this figure the corresponding ratio $q_T(\alpha_{opt}, N, m)$ and in the bottom graph the quantity $q_T(\alpha_{opt}, N, m)^N$ which indicates the exponential decay of the truncation errors TE as $N \to \infty$. All these graphs correspond to the values of $m = 3, 6, 9, 12, 15$ and 18. It can be verified that

$$\alpha_{opt}(N, m) \to \bar{\alpha}_{opt} = \frac{1}{2e} \approx 0.1839 \quad \text{as} \quad N \to \infty$$

for any m, where $\bar{\alpha}_{opt}$ corresponds to the minimum of the objective function

$$\bar{q}_T(\alpha) := \lim_{N\to\infty} q_T(\alpha, N, m) = (2\alpha)^\alpha$$

which is independent of m. Here, $q_T(\alpha, N, m)$ is defined by (3.1) and we have used the relation $\lim_{N\to\infty}(1+aN)^{1/N} = 1$, where a is an arbitrary real number. Therefore, this minimum value is $\bar{q}_T(\bar{\alpha}_{opt}) \approx 0.8320$. Observe also that

$$\bar{q}_T(\alpha) < 1 \quad \text{for} \quad \alpha < \frac{1}{2}.$$

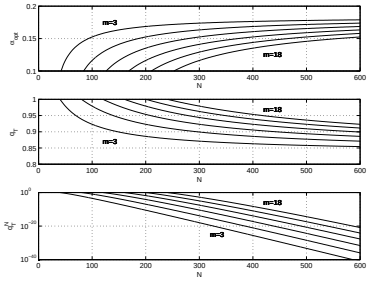

Figure 2. The quantities α_{opt}, $q_T(\alpha_{opt}, N, m)$ and $q_T(\alpha_{opt}, N, m)^N$ versus N for $m = 3, 6, 9, 12, 15$ and 18.

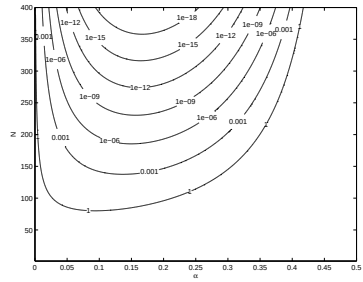

Figure 3. Contour plots of $q_T(\alpha, N, m)^N$ given by (3.2) for $m = 6$.

We have

$$q_T^N = q_T(\alpha, N, m)^N = \Big(1 + \frac{2\alpha N}{m}\Big)^m \Big(\frac{m}{N} + 2\alpha\Big)^{2\alpha N} \big(2\alpha\big)^{-\alpha N}, \tag{3.2}$$

which for large N is asymptotic to

$$q_T(\alpha, N, m)^N \sim \Big(1 + \frac{2\alpha N}{m}\Big)^m (2\alpha)^{\alpha N}.$$

Hence,

$$\lim_{N\to\infty} q_T(\alpha, N, m)^N = 0$$

for any m and $\alpha < 1/2$. The rate of convergence is very fast which is also illustrated in Fig. 3 by contour plots of $q_T(\alpha, N, m)^N$ given by (3.2) for $m = 6$. Here we note that the analytical determination of α_{opt}, which in turn successfully predicted the corresponding numerical results, is a welcome improvement over the nature of the problem in [20] where β_{opt} could only be determined numerically.

We consider next the behavior of q_R and q_R^N as $N \to \infty$. Substituting $\beta = m/N$ into $q_R = q_{R,1}$ defined by (2.9) we obtain

$$q_{R,1} = q_{R,1}(\alpha, N, m, r_0) = \Big(1 + \frac{2\alpha N}{m}\Big)^{\frac{m}{2N}} \Big(1 + \frac{m}{2\alpha N}\Big)^{\alpha} r_0^{\frac{m}{N}}, \tag{3.3}$$

and it follows that

$$\lim_{N\to\infty} q_{R,1}(\alpha, N, m, r_0) = 1$$

for any α, m, and r_0. We have also

$$q_{R,1}^N = q_{R,1}(\alpha, N, m, r_0)^N = \Big(1 + \frac{2\alpha N}{m}\Big)^{\frac{m}{2}} \Big(1 + \frac{m}{2\alpha N}\Big)^{\alpha N} r_0^m \tag{3.4}$$

and it follows that

$$\lim_{N\to\infty} q_{R,1}(\alpha, N, m, r_0)^N = \infty$$

for any α, m, and r_0, where the divergence is of polynomial rate.

The situation is somewhat more favorable for the regularization ratio $q_R = q_{R,2}$. Substituting $\beta = m/N$ into (2.11) we obtain

$$q_{R,2} = q_{R,2}(\alpha, N, m, \rho) = \frac{\left(\alpha + \frac{m}{2N}\right)^{\frac{m}{N}+2\alpha}}{\alpha^{\alpha}\left(\alpha + \frac{m}{N}\right)^{\frac{m}{N}+\alpha}\rho^{\frac{m}{N}}} \tag{3.5}$$

and it follows that

$$\lim_{N\to\infty} q_{R,2}(\alpha, N, m, \rho) = 1$$

for any α, m and ρ, the same limit as that for $q_{R,1}$ defined by (3.3). We have also

$$q_{R,2}^N = q_{R,2}(\alpha, N, m, \rho)^N = \frac{\left(\alpha + \frac{m}{2N}\right)^m \left(1 + \frac{m}{2\alpha N}\right)^{2\alpha N}}{\left(\alpha + \frac{m}{N}\right)^m \left(1 + \frac{m}{\alpha N}\right)^{\alpha N} \rho^m}$$

and passing with N to infinity we obtain

$$\lim_{N\to\infty} q_{R,2}(\alpha, N, m, \rho)^N = 1/\rho^m$$

for any α. This differs from the behavior observed for $q_{R,1}^N$ given by (3.4) for which $\lim_{N\to\infty} q_{R,1}^N \to \infty$ at polynomial rate. However, both error bounds in (2.6) and (2.7) tend to infinity as $N \to \infty$ since $A(N)$ and $\tilde{A}(N)$ have a polynomial growth with respect to N.

4 Strategies for Choosing Optimal Parameters Based on One-Dimensional Minimization

We first consider the case when $q_R = q_{R,1}$ is defined by (3.3). To obtain additional insight into the behavior of error bounds (2.6) and (2.7) for a fixed value of the parameter m, we have plotted in Fig. 4 the contour plots of $q_T^N + q_{R,1}^N$ for $m = 6$ and $r_0 = 0.1$, where q_T^N is given by (3.2) and $q_{R,1}^N$ is given by (3.4).

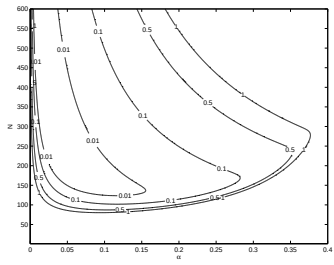

Figure 4. Contour plots of $q_T(\alpha, N, m)^N + q_{R,1}(\alpha, N, m, r_0)^N$ for $m = 6$ and $r_0 = 0.1$.

We have also plotted in Fig. 5 the cross-section of $q_T^N + q_{R,1}^N$ for fixed $N = 400$ and in Fig. 6 the cross-section of $q_T^N + q_{R,1}^N$ for fixed $\alpha = 0.1$ and for $m = 3, 6, 9, 12, 15$ and 18.

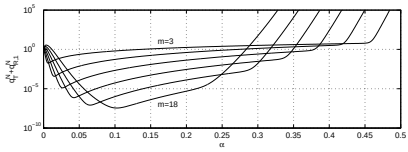

Figure 5. Cross-sections of $q_T(\alpha, N, m)^N + q_{R,1}(\alpha, N, m, r_0)^N$ for $N = 400$, $r_0 = 0.1$ and $m = 3, 6, 9, 12, 15$ and 18.

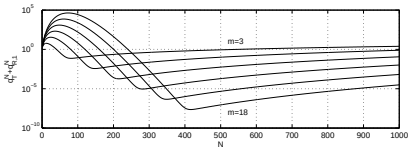

Figure 6. Cross-sections of $q_T(\alpha, N, m)^N + q_{R,1}(\alpha, N, m, r_0)^N$ for $\alpha = 0.1$, $r_0 = 0.1$ and $m = 3, 6, 9, 12, 15$ and 18.

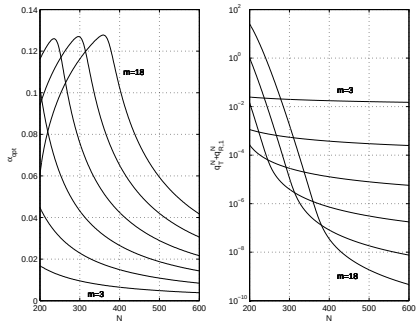

Figure 7. α_{opt} versus N (left graph) and $q_T^N + q_{R,1}^N$ versus N (right graph) for $r_0 = 0.1$ and $m = 3, 6, 9, 12, 15$ and 18.

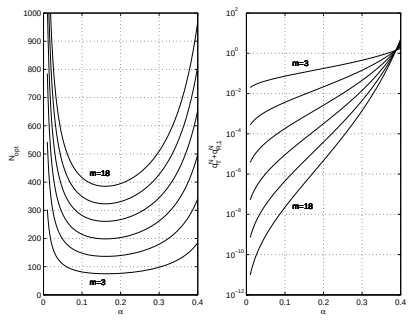

Figure 8. N_{opt} versus α (left graph) and $q_T^N + q_{R,1}^N$ versus α (right graph) for $r_0 = 0.1$ and $m = 3, 6, 9, 12, 15$ and 18.

The solutions obtained for α_{opt} are plotted on the left graph of Fig. 7 versus N and the corresponding quantities $q_T^N + q_{R,1}^N$ are plotted on the right graph of this figure for $200 \le N \le 600$. This figure corresponds to $r_0 = 0.1$ and $m = 3, 6, 9, 12, 15$ and 18. The solutions obtained for N_{opt} are plotted on the left graph of Fig. 8 versus α and the quantities $q_T^N + q_{R,1}^N$ are plotted on the right graph of this figure for $0 \le \alpha \le 0.4$. Again, this figure corresponds to $r_0 = 0.1$ and $m = 3, 6, 9, 12, 15$ and 18. For example, if $r_0 = 0.1$, $N = 400$ and $m = 3$ or $m = 18$ then it follows from Fig. 7 that $\alpha_{opt} \approx 0.007$ or $\alpha_{opt} \approx 0.1$ and $q_T^N + q_{R,1}^N \approx 1.8 \cdot 10^{-2}$ or $q_T^N + q_{R,1}^N \approx 3.5 \cdot 10^{-8}$. Similarly, if $r_0 = 0.1$, $\alpha = 0.2$ and $m = 3$ or $m = 18$ then it follows from Fig. 8 that $N_{opt} \approx 76$ or $N_{opt} \approx 400$ and $q_T^N + q_{R,1}^N \approx 1.8 \cdot 10^{-1}$ or $q_T^N + q_{R,1}^N \approx 4.8 \cdot 10^{-6}$.

These plots indicate that although the $q_T^N + q_{R,1}^N \to \infty$ as $N \to \infty$, it will reach quite small values before diverging to infinity. Hence, the Gegenbauer reconstruction is still of practical use. Our strategies for choosing optimal α for given N or choosing optimal N for given α are based on exploiting this behavior. For fixed m and r_0 , we consider the minimization problem

$$q_T(\alpha, N, m)^N + q_{R,1}(\alpha, N, m, r_0)^N \to \min, \tag{4.1}$$

which we solve with respect to α if N is given, or with respect to N if α is given.

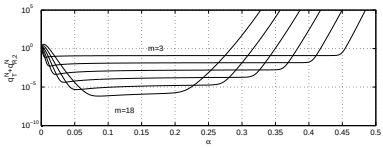

Figure 9. Cross-sections of $q_T(\alpha, N, m)^N + q_{R,2}(\alpha, N, m, \rho)^N$ for $N = 400$, $\rho = 2$ and $m = 3, 6, 9, 12, 15$ and 18.

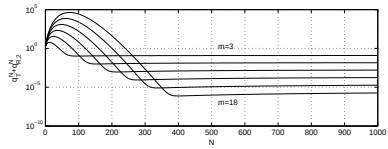

Figure 10. Cross-sections of $q_T(\alpha, N, m)^N + q_{R,2}(\alpha, N, m, \rho)^N$ for $\alpha = 0.1$, $\rho = 2$ and $m = 3, 6, 9, 12, 15$ and 18.

We consider next the case when $q_T = q_{R,2}$ is defined by (3.5). Fig. 9 displays the cross-sections of $q_T^N + q_{R,2}^N$ for fixed $N = 400$ and in Fig. 10 the cross-sections of $q_T^N + q_{R,2}^N$ for fixed $\alpha = 0.1$ and for $m = 3, 6, 9, 12, 15$ and 18. Both figures correspond to $\rho = 2$. We can observe that the minimum of $q_T^N + q_{R,2}^N$ for fixed N is quite flat for a large range of the parameter α and that the minimum of $q_T^N + q_{R,2}^N$ for fixed α is flat for $N \in [N_0, \infty]$, where $N_0 = N_0(\alpha)$ is some constant depending on α. Moreover, this minimum is only slightly smaller than the limit

$$\lim_{N\to\infty} \left(q_T^N + q_{R,2}^N\right) = \left(\frac{1}{\rho}\right)^m$$

computed in Section 3.

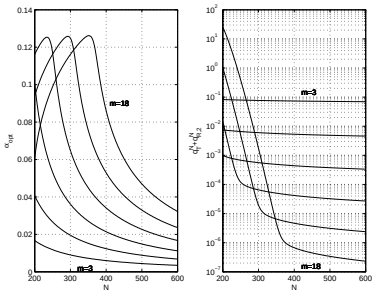

Figure 11. α_{opt} versus N (left graph) and $q_T^N + q_{R,2}^N$ versus N (right graph) for $\rho = 2$ and $m = 3, 6, 9, 12, 15$ and 18.

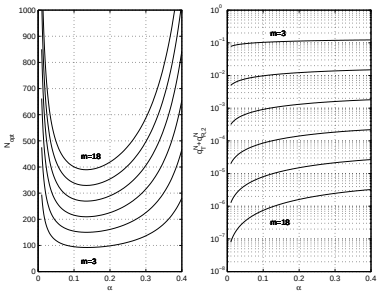

Figure 12. N_{opt} versus α (left graph) and $q_T^N + q_{R,2}^N$ versus α (right graph) for $\rho = 2$ and $m = 3, 6, 9, 12, 15$ and 18.

The strategy based on the one-dimensional minimization problem

$$q_T(\alpha, N, m)^N + q_{R,2}(\alpha, N, m, \rho)^N \to \min \tag{4.2}$$

still works and the solution of (4.2) for α_{opt} versus N is plotted in Fig. 11 and for N_{opt} versus α in Fig. 12. These figures correspond to $\rho = 2$ and $m = 3$,6, 9, 12, 15 and 18. For example, if $\rho = 2$, $N = 400$ and $m = 3$ or $m = 18$ then it follows from Fig. 11 that $\alpha_{opt} \approx 0.006$ or $\alpha_{opt} \approx 0.09$ and

$q_T^N + q_{R,2}^N \approx 7.4 \cdot 10^{-2}$ or $q_T^N + q_{R,2}^N \approx 6.7 \cdot 10^{-7}$. Similarly, if $\rho = 2$, $\alpha = 0.2$ and $m = 3$ or $m = 18$ then it follows from Fig. 12 that $N_{opt} \approx 99$ or $N_{opt} \approx 420$ and $q_T^N + q_{R,2}^N \approx 1.1 \cdot 10^{-1}$ or $q_T^N + q_{R,2}^N \approx 1.6 \cdot 10^{-6}$.

5 Strategies for Choosing Optimal Parameters Based on Two-Dimensional Minimization

In this section we describe a strategy for choosing optimal parameters α and N for given r_0 and m. This strategy is an adaptation of the one developed in [10] and [19] for choosing optimal parameters α and β, $\lambda = \alpha N$, $m = \beta N$, where λ as well as m were allowed to grow proportionally with the number of Fourier modes N.

Consider first the case where $q_R = q_{R,1}$ is given by (3.3). Similarly, as in [10, 19], our strategy is based on minimizing the objective function defined by

$$\phi_1(\alpha, N, m, r_0) := q_T(\alpha, N, m) + K\Big(q_T(\alpha, N, m) - q_{R,1}(\alpha, N, m, r_0)\Big)^2, \quad (5.1)$$

where m and r_0 are given parameters, and $K > 0$ is a penalty constant. Solving the two-dimensional minimization problem

$$\phi_1(\alpha, N, m, r_0) \to \min \quad (5.2)$$

for given m and r_0 with respect to α and N for large penalty constant K (we have chosen $K = 100$ in our numerical experiments) amounts to enforcing approximately equal contributions to the global error bound of Gegenbauer reconstruction from the truncation error TE in (2.6) and represented by the ratio $q_T(\alpha, N, m)$, and regularization error RE in (2.7) represented by the ratio $q_{R,1}(\alpha, N, m, r_0)$.

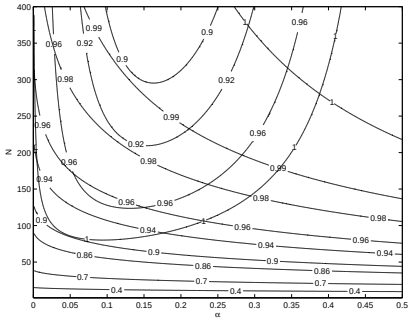

Figure 13. Contour plots of $q_T(\alpha, N, m)$ given by (3.1) and $q_{R,1}(\alpha, N, m, r_0)$ given by (3.3) for $r_0 = 0.1$ and $m = 6$.

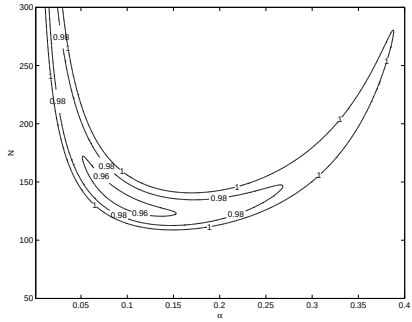

Figure 14. Contour plots of the objective function $\phi_1(\alpha, N, m, r_0)$ given by (5.1) for $r_0 = 0.1$, $m = 6$ and $K = 100$.

One may suspect that the minimization problem (5.2) will lead only to the 'singular solution' $\alpha = 0$ and $N = \infty$. This is not the case. It turns out that the problem (5.2) has a local minimum. This is illustrated by contour plots of $q_T(\alpha, N, m)$ and $q_{R,1}(\alpha, N, m, r_0)$ displayed in Fig. 13 and contour

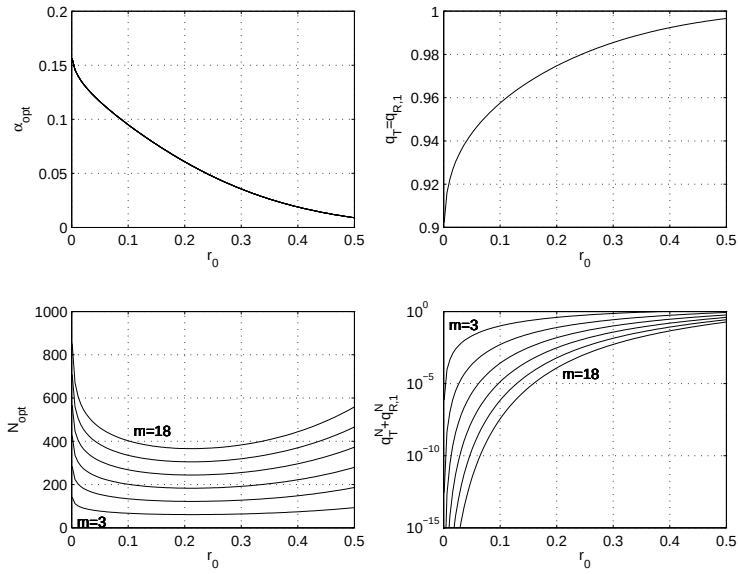

Figure 15. α_{opt} versus r_0 (top left graph), N_{opt} versus r_0 (bottom left graph), $q_T = q_{R,1}$ versus r_0 (top right graph) and $q_T^N + q_{R,1}^N$ versus r_0 (bottom right graph) for $m = 3, 6, 9, 12, 15$ and 18.

plots of objective function $\phi_1(\alpha, N, m, r_0)$ defined by (5.1) displayed in Fig. 14. These contour plots correspond to $r_0 = 0.1$ and $m = 6$. Observe that the local minimum corresponds to the point on Fig. 13 where the contour lines for $q_T(\alpha, N, m)$ and $q_{R,1}(\alpha, N, m, r_0)$ are tangent for the same value of $q_T = q_{R,1}$. Note also that the local minimum of the objective function $\phi_1(\alpha, N, m, r_0)$ for $m = 6$ and $r_0 = 0.1$ corresponds to a point in Fig. 14 inside of the contour line with the value of 0.96.

We have solved the minimization problem (5.2) for $m = 3, 6, 9, 12, 15$ and 18 and the parameter $r_0 \in [0, 0.5]$. The graph of α_{opt} versus r_0 is displayed in the top left graph of Fig. 15 and N_{opt} versus r_0 in the bottom left graph of this figure. It is interesting to note that α_{opt} is nearly independent of m. We have also plotted $q_T = q_{R,1}$ in the top right graph of Fig. 15 and $q_T^N + q_{R,1}^N$ in the bottom right graph of this figure. Observe that the error bound for Gegenbauer reconstruction for fixed m deteriorates rapidly as the smoothness parameter r_0 becomes larger.

The values of the optimal parameters α_{opt} and N_{opt} obtained by the solution to the minimization problem (5.2) are consistent with the values obtained by the one-dimensional minimization discussed in Section 4. For example, for $r_0 = 0.1$ and $m = 18$ the solution to (5.2) is $\alpha_{opt} \approx 0.0943$ and $N_{opt} \approx 401$ with the corresponding values of $q_T = q_{R,1} \approx 0.9579$ and $q_T^N + q_{R,1}^N \approx 4.51 \cdot 10^{-8}$. Solving instead the problem (4.1) for $r_0 = 0.1$, $m = 18$ and $N = 401$ we obtain $\alpha_{opt} \approx 0.1017$ with corresponding values of $q_T \approx 0.9564$, $q_{R,1} \approx 0.9563$, and $q_T^N + q_{R,1}^N \approx 3.34 \cdot 10^{-8}$ which are nearly equivalent to the values obtained by

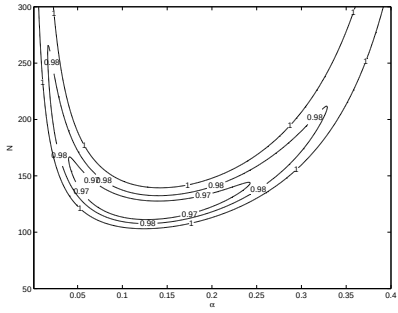

Figure 16. Contour plots of the objective function $\phi_2(\alpha, N, m, \rho)$ given by (5.3) for $\rho = 2$, $m = 6$ and $K = 100$.

the solution to (5.2). Solving (4.1) for $r_0 = 0.1$, $m = 18$, and $\alpha = 0.0943$, we obtain $N_{opt} \approx 423$ with corresponding values of $q_T \approx 0.9541$, $q_{R,1} \approx 0.9582$, and $q_T^N + q_{R,1}^N \approx 1.61 \cdot 10^{-8}$ which are again quite close to the values obtained by the solution to (5.2).

Consider next the case where $q_T = q_{R,2}$ given by (3.5). We define the objective function

$$\phi_2(\alpha, N, m, \rho) := q_T(\alpha, N, m) + K\Big(q_T(\alpha, N, m) - q_{R,2}(\alpha, N, m, \rho)\Big)^2, \quad (5.3)$$

where m and ρ are given parameters and $K > 0$ is a penalty constant. The level curves of $\phi_2(\alpha, N, m, \rho)$ defined by (5.3) are plotted on Fig. 16 for $\rho = 2$ and $m = 6$. This figure illustrates that $\phi_2(\alpha, N, m, \rho)$ has a local minimum. We then consider the two-dimensional minimization problem

$$\phi_2(\alpha, N, m, \rho) \to \min. \quad (5.4)$$

We solve (5.4) with respect to α and N for given m and ρ, specifically, for $m = 3, 6, 9, 12, 15$ and 18 and the parameter $\rho \in [1, 6]$. The graph of α_{opt} versus ρ is displayed in the top left graph of Fig. 17 and N_{opt} versus ρ in the bottom left graph of this figure. As before we observe that α_{opt} is nearly independent of m. We have also plotted $q_T = q_{R,2}$ in the top right graph of Fig. 17 and $q_T^N + q_{R,2}^N$ in the bottom right graph of this figure. We can observe that the error bound for Gegenbauer reconstruction for fixed m improves as the parameter ρ becomes larger.

Similarly, as in the case of (5.2), the values of the optimal parameters α_{opt} and N_{opt} obtained by the solution to the minimization problem (5.4) are consistent with the values obtained by the one-dimensional minimization discussed in Section 4. For example, for $\rho = 2$ and $m = 18$ the solution to (5.4) is $\alpha_{opt} \approx 0.1170$ and $N_{opt} \approx 359$ with the corresponding values of $q_T = q_{R,2} \approx 0.9632$ and $q_T^N + q_{R,2}^N \approx 2.20 \cdot 10^{-6}$. Solving instead the problem (4.2) for $\rho = 2$, $m = 18$ and $N = 359$ we obtain $\alpha_{opt} \approx 0.1253$ with corresponding values of $q_T \approx 0.9628$, $q_{R,2} \approx 0.9618$, and $q_T^N + q_{R,2}^N \approx 2.01 \cdot 10^{-6}$ which are nearly equivalent to the values obtained by the solution to (5.4). Solving (4.2)

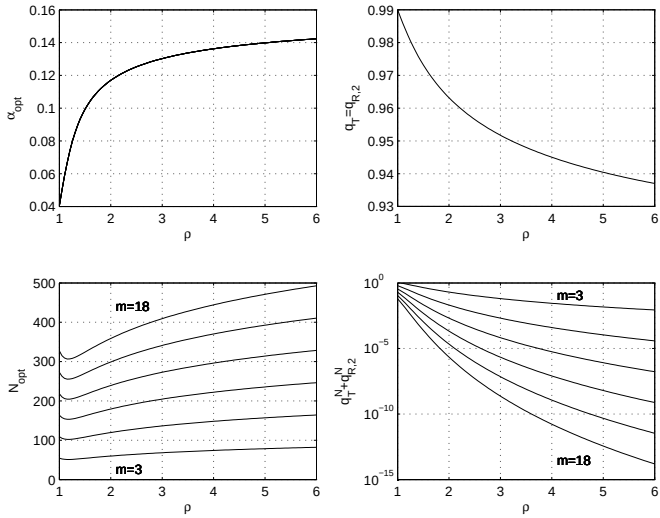

Figure 17. α_{opt} versus ρ (top left graph), N_{opt} versus ρ (bottom left graph), $q_T = q_{R,1}$ versus ρ (top right graph) and $q_T^N + q_{R,2}^N$ versus ρ (bottom right graph) for $m = 3, 6, 9, 12, 15$ and 18.

for $\rho = 2$, $m = 18$ and $\alpha = 0.1170$ we obtain $N_{opt} \approx 392$ with corresponding values of $q_T \approx 0.9560$, $q_{R,2} \approx 0.9550$, and $q_T^N + q_{R,2}^N \approx 8.94 \cdot 10^{-7}$ which are again close to the values obtained by the solution to (5.4).

6 Numerical Experiments

6.1 One-dimensional test functions

In this section we numerically test the effectiveness of our strategies for determining the optimal parameters α_{opt} and N_{opt}. For this purpose we will use functions which have singularities on the imaginary and on the real axis. These functions are defined by

$$f(x) = \begin{cases} \dfrac{e^x}{x^2 + \rho^2}, & -\frac{1}{2} \le x \le \frac{1}{2}, \\ 0, & \text{otherwise}, \end{cases} \tag{6.1}$$

with singularities on the imaginary axis at $x = \pm\rho i$, and

$$f(x) = \begin{cases} \dfrac{e^x}{x^2 - (1+\rho)^2}, & -\frac{1}{2} \le x \le \frac{1}{2}, \\ 0, & \text{otherwise}, \end{cases} \tag{6.2}$$

with singularities on the real axis at $x = \pm(1 + \rho)$. It is easy to verify that these functions satisfy the condition (2.10), and that ρ is the distance from the interval $[-1, 1]$ to the nearest singularity of $f(x)$ in the complex plane.

We compute α_{opt} and N_{opt} by solving the problem (5.2) or (5.4) for given m and r_0 or m or ρ, respectively. It was demonstrated in [10] that the relationships between the parameter r_0 appearing in (2.9) and ρ are

$$\rho = \frac{1}{2}\left(\frac{1}{r_0} - r_0\right) \quad \text{or} \quad r_0 = \sqrt{1+\rho^2} - \rho$$

if $f(x)$ is defined by (6.1), and

$$\rho = \frac{(r_0-1)^2}{2r_0} \quad \text{or} \quad r_0 = 1 + \rho - \sqrt{\rho^2 + 2\rho}$$

if $f(x)$ is defined by (6.2). The optimal values of the parameters α and N obtained by the minimization of (5.2) with $f(x)$ defined by (6.1) are denoted by $\alpha_{opt,I}$ and $N_{opt,I}$, and the values obtained by the solution of (5.2) with $f(x)$ defined by (6.2) are denoted by $\alpha_{opt,R}$ and $N_{opt,R}$. Here, I and R signify imaginary and real. Similarly, the corresponding values of α and N obtained by the minimization of (5.4) for $f(x)$ defined by (6.1) or (6.2) are denoted by $\alpha_{opt,\rho}$ and $N_{opt,\rho}$. The values of $\alpha_{opt,\rho}$, $\alpha_{opt,I}$ and $\alpha_{opt,R}$ are listed in Table 1 for $\rho = 1, 2, 3, 4, 5$ and 6 together with the corresponding values of the parameter r_0 which are denoted by $r_{0,I}$ if $f(x)$ is given by (6.1) and $r_{0,R}$ if $f(x)$ is defined by (6.2). It is interesting that $\alpha_{opt,\rho}$, $\alpha_{opt,I}$ and $\alpha_{opt,R}$ are all nearly independent of the parameter m.

Table 1. Optimal parameters $\alpha_{opt,\rho}$, $\alpha_{opt,I}$ and $\alpha_{opt,R}$ corresponding to ρ and r_0.

ρ	1	2	3	4	5	6
$r_{0,I}$	0.4142	0.2361	0.1623	0.1231	0.0990	0.0828
$r_{0,R}$	0.2679	0.1716	0.1270	0.1010	0.0839	0.0718
$\alpha_{opt,\rho}$	0.0406	0.1170	0.1303	0.1363	0.1399	0.1423
$\alpha_{opt,I}$	0.0171	0.0506	0.0726	0.0862	0.0954	0.1019
$\alpha_{opt,R}$	0.0426	0.0696	0.0848	0.0946	0.1014	0.1065

Table 2. Optimal parameters $N_{opt,\rho}$, $N_{opt,I}$ and $N_{opt,R}$ corresponding to ρ and r_0.

ρ		1	2	3	4	5	6
$m = 6$	$N_{opt,\rho}$	109	120	136	148	157	164
	$N_{opt,I}$	152	122	124	129	134	139
	$N_{opt,R}$	124	123	128	134	139	143
$m = 12$	$N_{opt,\rho}$	218	239	273	296	314	328
	$N_{opt,I}$	304	245	248	258	269	278
	$N_{opt,R}$	249	247	257	268	278	286
$m = 18$	$N_{opt,\rho}$	327	359	409	444	471	493
	$N_{opt,I}$	457	367	372	387	403	417
	$N_{opt,R}$	373	370	385	401	416	430

The corresponding values of $N_{opt,\rho}$, $N_{opt,I}$ and $N_{opt,R}$ depend on m and are listed in Table 2 for $m = 6$, 12 and 18. The errors of the Gegenbauer reconstruction of the function $f(x)$ defined by (6.1) are displayed in Fig. 18 for $\rho = 1$, 2, and 4, and $m = 6$, 12, and 18, with parameters $\alpha_{opt,I}$, $N_{opt,I}$ (solid lines) and $\alpha_{opt,\rho}$, $N_{opt,\rho}$ (dashed lines). The corresponding errors for $f(x)$ defined by (6.2) are displayed in Fig. 19.

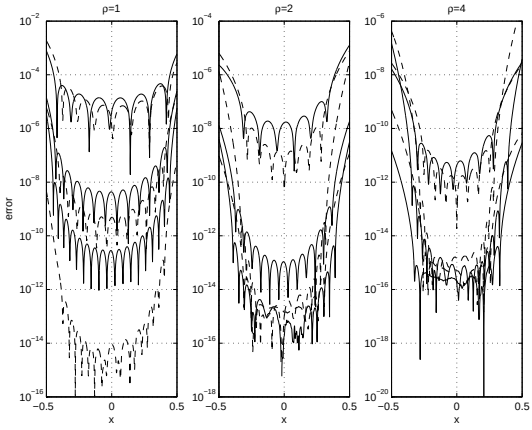

Figure 18. Errors for the Gegenbauer reconstruction of the function $f(x)$ defined by (6.1) for $\rho = 1$, 2, and 4 and $m = 6$, 12, and 18, with parameters $\alpha_{opt,I}$, $N_{opt,I}$ (solid lines) and $\alpha_{opt,\rho}$, $N_{opt,\rho}$ (dashed lines). These parameters are listed in Table 1 and Table 2.

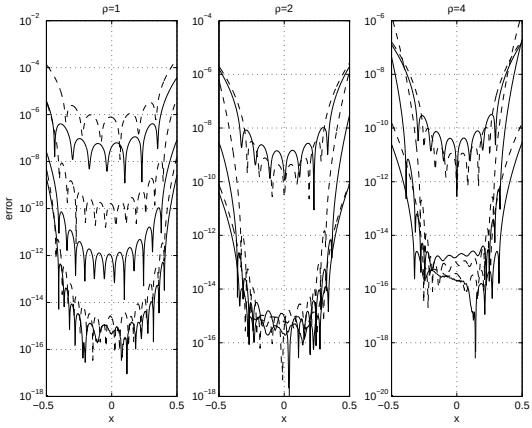

Figure 19. Errors for the Gegenbauer reconstruction of the function $f(x)$ defined by (6.2) for $\rho = 1$, 2, and 4 and $m = 6$, 12, and 18, with parameters $\alpha_{opt,R}$, $N_{opt,R}$ (solid lines) and $\alpha_{opt,\rho}$, $N_{opt,\rho}$ (dashed lines); these parameters are listed in Table 1 and Table 2.

These errors are also listed in Table 3 and Table 4, identified as $E(N)$, for $f(x)$ defined by (6.1) and for the parameters $\alpha_{opt,I}$, $N_{opt,I}$ and $\alpha_{opt,\rho}$, $N_{opt,\rho}$,

respectively. In these tables we have also listed the quantities $B(N)$ and $C(N)$ such that

$$E(N) := \|f - f_g^{m,\lambda}\|_\infty \le C(N)B(N), \tag{6.3}$$

where

$$B(N) = q_T^N + q_{R,i}^N, \quad i = 1, 2, \quad C(N) = \max\Big\{A(N), \tilde{A}(N)\Big\},$$

with $A(N)$ and $\tilde{A}(N)$ defined in (2.6) and (2.7).

Table 3. $E(N)$, $B(N)$ and $C(N)$ corresponding to $\alpha_{opt,I}$, $N_{opt,I}$ for $f(x)$ from (6.1).

ρ		1	2	4
$m = 6$	$E(N)$	$7.75 \cdot 10^{-4}$	$1.27 \cdot 10^{-5}$	$2.92 \cdot 10^{-8}$
	$B(N)$	$5.92 \cdot 10^{-1}$	$1.36 \cdot 10^{-1}$	$1.22 \cdot 10^{-2}$
	$C(N)$	$1.31 \cdot 10^{-3}$	$9.34 \cdot 10^{-5}$	$2.39 \cdot 10^{-6}$
$m = 12$	$E(N)$	$2.46 \cdot 10^{-5}$	$1.85 \cdot 10^{-8}$	$2.87 \cdot 10^{-11}$
	$B(N)$	$1.81 \cdot 10^{-1}$	$9.08 \cdot 10^{-3}$	$7.67 \cdot 10^{-5}$
	$C(N)$	$1.34 \cdot 10^{-4}$	$2.04 \cdot 10^{-6}$	$3.74 \cdot 10^{-7}$
$m = 18$	$E(N)$	$5.57 \cdot 10^{-6}$	$4.08 \cdot 10^{-9}$	$1.50 \cdot 10^{-7}$
	$B(N)$	$5.71 \cdot 10^{-2}$	$6.28 \cdot 10^{-4}$	$4.91 \cdot 10^{-7}$
	$C(N)$	$9.75 \cdot 10^{-5}$	$6.50 \cdot 10^{-6}$	$3.05 \cdot 10^{-1}$

Table 4. $E(N)$, $B(N)$ and $C(N)$ corresponding to $\alpha_{opt,\rho}$, $N_{opt,\rho}$ for $f(x)$ from (6.1).

ρ		1	2	4
$m = 6$	$E(N)$	$1.86 \cdot 10^{-3}$	$7.79 \cdot 10^{-6}$	$2.73 \cdot 10^{-8}$
	$B(N)$	$6.21 \cdot 10^{-1}$	$2.04 \cdot 10^{-2}$	$3.96 \cdot 10^{-4}$
	$C(N)$	$3.00 \cdot 10^{-3}$	$3.82 \cdot 10^{-4}$	$6.89 \cdot 10^{-5}$
$m = 12$	$E(N)$	$1.84 \cdot 10^{-5}$	$1.18 \cdot 10^{-9}$	$4.90 \cdot 10^{-10}$
	$B(N)$	$1.94 \cdot 10^{-1}$	$2.11 \cdot 10^{-4}$	$8.06 \cdot 10^{-8}$
	$C(N)$	$9.48 \cdot 10^{-5}$	$5.59 \cdot 10^{-6}$	$6.08 \cdot 10^{-3}$
$m = 18$	$E(N)$	$6.17 \cdot 10^{-8}$	$2.95 \cdot 10^{-6}$	$1.50 \cdot 10^{-7}$
	$B(N)$	$6.10 \cdot 10^{-2}$	$2.20 \cdot 10^{-6}$	$1.68 \cdot 10^{-11}$
	$C(N)$	$1.01 \cdot 10^{-6}$	$1.34 \cdot 10^{0}$	$8.93 \cdot 10^{3}$

The errors corresponding to $f(x)$ defined by (6.2) are listed in Table 5 and Table 6 for the parameters $\alpha_{opt,R}$, $N_{opt,R}$ and $\alpha_{opt,\rho}$, $N_{opt,\rho}$, respectively. As before, we have also listed the quantities $B(N)$ and $C(N)$, and have computed $C(N)$ as the ratio of $E(N)$ to $B(N)$.

Analyzing the results presented in Figs. 18–19, and in the Tables 3–6, we observe that the Gegenbauer reconstruction with the parameters $\alpha_{opt,I}$, $N_{opt,I}$ or $\alpha_{opt,R}$, $N_{opt,R}$ obtained by minimization of (5.2) leads, in most cases, to somewhat more accurate results than the reconstruction with the parameters $\alpha_{opt,\rho}$, $N_{opt,\rho}$ obtained by minimization of (5.4). On the other hand, the errors

Table 5. $E(N)$, $B(N)$ and $C(N)$ corresponding to $\alpha_{opt,R}$, $N_{opt,R}$ for $f(x)$ from (6.2).

ρ		1	2	4
$m=6$	$E(N)$	$3.77 \cdot 10^{-5}$	$1.96 \cdot 10^{-6}$	$1.58 \cdot 10^{-7}$
	$B(N)$	$1.96 \cdot 10^{-1}$	$4.47 \cdot 10^{-2}$	$5.33 \cdot 10^{-3}$
	$C(N)$	$1.92 \cdot 10^{-4}$	$4.38 \cdot 10^{-5}$	$2.96 \cdot 10^{-5}$
$m=12$	$E(N)$	$8.38 \cdot 10^{-8}$	$8.02 \cdot 10^{-11}$	$2.90 \cdot 10^{-11}$
	$B(N)$	$1.97 \cdot 10^{-2}$	$1.02 \cdot 10^{-3}$	$1.46 \cdot 10^{-5}$
	$C(N)$	$4.25 \cdot 10^{-6}$	$7.86 \cdot 10^{-8}$	$1.99 \cdot 10^{-6}$
$m=18$	$E(N)$	$2.61 \cdot 10^{-9}$	$3.02 \cdot 10^{-8}$	$2.01 \cdot 10^{-7}$
	$B(N)$	$2.00 \cdot 10^{-3}$	$2.37 \cdot 10^{-5}$	$4.08 \cdot 10^{-8}$
	$C(N)$	$1.31 \cdot 10^{-6}$	$1.27 \cdot 10^{-3}$	$4.93 \cdot 10^{0}$

Table 6. $E(N)$, $B(N)$ and $C(N)$ corresponding to $\alpha_{opt,\rho}$, $N_{opt,\rho}$ for $f(x)$ from (6.2).

ρ		1	2	4
$m=6$	$E(N)$	$2.29 \cdot 10^{-4}$	$2.63 \cdot 10^{-6}$	$1.94 \cdot 10^{-7}$
	$B(N)$	$6.21 \cdot 10^{-1}$	$2.04 \cdot 10^{-2}$	$3.96 \cdot 10^{-4}$
	$C(N)$	$3.69 \cdot 10^{-4}$	$1.29 \cdot 10^{-4}$	$4.90 \cdot 10^{-4}$
$m=12$	$E(N)$	$5.15 \cdot 10^{-8}$	$8.77 \cdot 10^{-11}$	$1.59 \cdot 10^{-10}$
	$B(N)$	$1.94 \cdot 10^{-1}$	$2.11 \cdot 10^{-4}$	$8.06 \cdot 10^{-8}$
	$C(N)$	$2.65 \cdot 10^{-7}$	$4.16 \cdot 10^{-7}$	$1.97 \cdot 10^{-3}$
$m=18$	$E(N)$	$1.63 \cdot 10^{-8}$	$1.32 \cdot 10^{-6}$	$2.01 \cdot 10^{-6}$
	$B(N)$	$6.10 \cdot 10^{-2}$	$2.20 \cdot 10^{-6}$	$1.68 \cdot 10^{-11}$
	$C(N)$	$2.67 \cdot 10^{-7}$	$6.00 \cdot 10^{-1}$	$1.19 \cdot 10^{5}$

corresponding to reconstruction with $\alpha_{opt,\rho}$, $N_{opt,\rho}$ are, in general, somewhat smaller in the middle of the interval $[-1, 1]$ than the errors corresponding to reconstruction with $\alpha_{opt,I}$, $N_{opt,I}$ or $\alpha_{opt,R}$, $N_{opt,R}$. We can also observe that the actual errors of the Gegenbauer reconstruction, $E(N)$, are only a fraction of the quantities $B(N)$ appearing in the error bound (6.3). This is signified by the values of $C(N) = E(N)/B(N)$ in Tables 3–6.

Tables 3–6 also indicate somewhat irregular behavior in the errors of the Gegenbauer reconstruction for $m = 18$. We can observe that, contrary to the cases of $m = 6$ and $m = 12$, the errors corresponding to $\rho = 4$ are larger than the errors corresponding to $\rho = 2$. This is due to the influence of round-off errors which become dominant for large values of the parameter $\lambda_{opt} = \alpha_{opt} N_{opt}$. This parameter for $m = 18$ and $\rho = 4$ has the values $\lambda_{opt,I} = \alpha_{opt,I} N_{opt,I} = 33.36$ and $\lambda_{opt,\rho} = \alpha_{opt,\rho} N_{opt,\rho} = 60.52$ if the function $f(x)$ is defined by (6.1) and $\lambda_{opt,R} = \alpha_{opt,R} N_{opt,R} = 37.93$ and $\lambda_{opt,\rho} = \alpha_{opt,\rho} N_{opt,\rho} = 60.52$ if $f(x)$ is defined by (6.2), compare Tables 1– 2.

The influence of round-off errors for the Gegenbauer reconstruction was investigated in [4, 9, 11] and helps to explain the above results. Although the Gegenbauer reconstruction method provides a means to avoid Gibbs phe-

nomenon, its use is not without cost. As described in the Section 2, spectral convergence of a Gegenbauer reconstruction requires that λ and m depend linearly on N. But as N, and thus λ, grows, round-off error encroaches upon the reconstruction error described above.

At first glance, an increase in λ appears to offer positive benefits. After all, higher powers on the weight function in (2.3) and (2.4) lead to smoother connections between periodic extensions of the original function and likewise between periodic extensions of the higher derivatives. Such periodicity explains the spectral accuracy of the Fourier coefficients from a periodic function as shown in [5, 12, 18]. Similarly this would appear to result in Gegenbauer coefficients that decay more quickly than those computed with lower values of λ. However, it was pointed out in [4, 11] that as λ increases, the weight function narrows and the reconstruction becomes more extrapolatory. That is, it depends more on the behavior of the original function central to the sampled interval to predict what it will do closer to the boundaries. At the same time, the narrowing weight function is also responsible for the significant increase in magnitude for all associated orders of Gegenbauer polynomials. Naturally the coefficients corresponding to such large polynomial basis functions must now carry their valued information at very small magnitudes. Then during reconstruction, multiplication of the very large with the very small leads to round-off error as shown in [9, 11].

In Section 7 we will explore these same parameter selection strategies given sample data taken from Fourier-Galerkin and collocation expansions.

6.2 Two-dimensional reconstruction

Previous studies, such as [2, 3, 20] have shown the effectiveness of performing Gegenbauer reconstructions on two-dimensional images, defined, of course, on evenly spaced grid points. In such cases the source data was understood to be from frequency space and hence, one- dimensional Fourier-Gegenbauer reconstructions were performed on each vertical column, or horizontal row, of data. This paper has, however, focused on Chebyshev-Gegenbauer reconstructions whose source data is understood to be defined on Gauss-Lobatto quadrature points, not a common image format. Nevertheless, we recognize the ability of a two-dimensional image to immediately convey a visceral sense of effectiveness for a given method of reconstruction. For this reason, and in the interest of continuity between studies, we also present a two-dimensional image reconstructed by the Chebyshev-Gegenbauer method.

As in prior studies, we chose to reconstruct the Shepp-Logan brain phantom, which is commonly used to compare the relative merits of medical image processing algorithms. This phantom is comprised of piecewise-smooth segments intended to model regions of similar tissue types whose densities are discontinuous with those in adjacent regions. Since it is defined algebraically, we sampled it on vertical, or horizontal, lines at Gauss-Lobatto quadrature points and subsequently projected this physical data into Chebyshev space. It was then a simple matter to re-expand the image as a finite Chebyshev series on equidistant grid points. The result is shown in Fig. 20 with, as expected,

Gibbs artifacts.

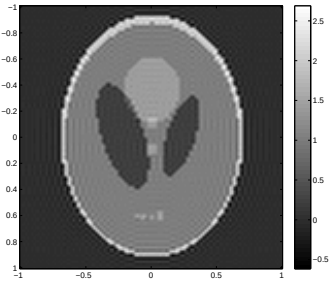

Figure 20. Chebyshev reconstruction of the Shepp-Logan brain phantom on [128 × 128] uniformly spaced grid points.

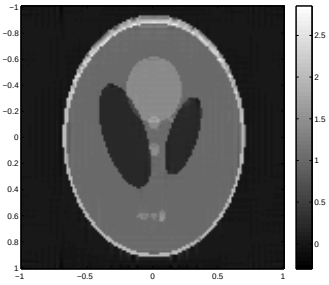

Figure 21. Gegenbauer reconstruction of the Shepp-Logan brain phantom on [128 × 128] uniformly spaced grid points using a dynamic selection of the reconstruction parameters and resulting in an 89% reduction in size over the original image.

We pause to note here that Section 5 in this paper assumed analyticity measure, ρ or r_0, and the number of Gegenbauer coefficients m to be among a preselected set of discrete convenient numbers. We then sought the optimal values of parameters α and N yielding the lowest apriori upper error bound. Using this approach we were able to find and present the correspondingly recommended, but still discrete, parameters α_{opt} and N_{opt}. There are however, times when, as in Section 4, we presuppose, or are given, a measure of analyticity in the form of ρ or r_0, as well as the value of N while we seek optimum values of both α and m to yield the lowest apriori upper error bound. Furthermore, the given parameters may fall between the discrete values selected in Section 4. Fortunately, [21] used the same ideas presented herein to develop closed form functions with which to treat such cases.

Returning now to the unmodified reconstruction of the Shepp-Logan phantom shown in Fig. 20, we seek not just a way to avoid Gibbs artifacts, but also a way to minimize the value of m, i.e. maximal compression, during a reconstruction where both analyticity and N are given. To achieve this we chose to perform a Chebyshev-Gegenbauer reconstruction on each vertical, or horizontal, line of Chebyshev coefficients used to recreate Fig. 20. But in order to do this, we first need to know the locations of the discontinuities in each line of data. Since we are not aware of a method to locate the physical discontinuities from the Chebyshev coefficients, we used the concentration edge detector in Fourier space, as described in [3, 6], to locate the intervals of smoothness. Subsequently we applied the Chebyshev-Gegenbauer method, dynamically choosing optimal parameters as described in the paragraph above, and also by [21]. In this way the value of N could be a variable integer based on the length of each smooth sub-domain.

The result, shown in Fig. 21, is clearly a significant improvement over the Chebyshev reconstruction shown in Fig. 20. By itself, this result does

not obviate the value of other reconstruction methods, such as total value regularization (TVR), which do not require an edge detection step and thus appear computationally cheaper. However, unlike the Chebyshev-Gegenbauer method, TVR requires an iterative minimization step. Moreover, unlike a TVR, this Gegenbauer reconstruction was able to compress the Chebyshev data to 11% of it's original size prior to reconstruction.

7 Gegenbauer Method Error Bounds Given Fourier or Pseudospectral Data

In Section 2 we pointed out that given the necessary relationship between α, β and N, both truncation and regularization errors tend to zero as the number of Chebyshev modes N tends to infinity. Subsequent sections then described strategies for selecting optimum parameters used to reconstruct a function from its Chebyshev series expansion. If, however, the source of f_N in (2.3) is a Fourier partial expansion such that

$$f_N(x) = \sum_{n=-N}^{N} \hat{f}_n e^{in\pi x}, \tag{7.1}$$

where the exact Fourier coefficients $\hat{f}_n$ are defined as

$$\hat{f}_n = \frac{1}{2}\int_{-1}^{1} f(x)e^{-in\pi x}dx, \quad n = -N, -N+1, \ldots, N, \tag{7.2}$$

then q_T, originally defined in (2.8), was instead shown in [15] to be

$$q_T = q_{TF} := \frac{(\beta + 2\,\alpha)^{\beta+2\,\alpha}}{(2\pi e\alpha)^{\alpha}\beta^{\beta}}. \tag{7.3}$$

Alternatively, if the data we possess for f_N came from a collocation expansion in either a Fourier or a general Gegenbauer spectral series, the ratio q_T was shown in [14, 15] to be

$$q_T = q_{TC} := \frac{(\beta + 2\,\alpha)^{\beta+2\,\alpha}}{(e\alpha)^{\alpha}\beta^{\beta}} \left(\frac{1}{2} + \frac{1}{4\rho}\right), \tag{7.4}$$

where ρ is the same measure of analyticity defined in (2.10).

Since a source for f_N other than the Chebyshev expansion considered in Sections 2–6 does not change the regularization error, analysis of the reconstruction error for these two additional circumstances can rely upon the same expressions for q_R presented in Sections 2 and 3. Then following the same analytical optimization described in Section 3, we find the expressions of optimum α given either of the two new expressions of q_T and any value of m as summarized, with the results from Section 3, in Table 7. Note also that analyticity parameters $r_{0,I}$ and $r_{0,R}$ in Table 7 are defined in Section 2.

The analytical results predicted in Table 7 indicate that when $q_T = q_{TC}$, we expect α_{opt} to be roughly twice the value of α_{opt} when $q_T = q_{TG}$. Table 7 also

Table 7. Comparison of $\bar{\alpha}_{opt}$, $\bar{q}_T(\alpha)$ and $\bar{q}_T(\bar{\alpha}_{opt})$ corresponding to expressions for q_T.

q_T (eqn)	ρ	$r_{0,I}$	$r_{0,R}$	$\bar{\alpha}_{opt}$	$\bar{q}_T(\alpha)$	$\bar{q}_T(\bar{\alpha}_{opt})$
q_{TG} (2.8)	-	-	-	$\frac{1}{2e}$	$(2\alpha)^{\alpha}$	0.8320
q_{TF} (7.3)	-	-	-	$\frac{\pi}{2}$	$\left(\frac{2\alpha}{\pi e}\right)^{\alpha}$	0.2079
q_{TC} (7.4)	$\frac{1}{2}$	$\frac{\sqrt{5}-1}{2}$	$\frac{3-\sqrt{5}}{2}$	$\frac{\rho}{2\rho+1} =$	$\frac{1}{4}$	0.7788
	1	$\sqrt{2}-1$	$2-\sqrt{3}$		$\frac{1}{3}$ $\left(\frac{\alpha(2\rho+1)}{e\rho}\right)^{\alpha}$	0.7165
	2	$\sqrt{5}-2$	$3-2\sqrt{2}$		$\frac{2}{5}$	0.6703
	4	$\sqrt{17}-4$	$5-\sqrt{24}$		$\frac{4}{9}$	0.6412

shows that when $q_T = q_{TF}$, we expect α_{opt} to be roughly one order of magnitude larger than α_{opt} when $q_T = q_{TG}$. The numerical experiments performed in [21] confirm these expectations. When $q_T = q_{TC}$, α_{opt} was found to be roughly twice the size, and N_{opt} to be roughly half the size of the same values when $q_T = q_{TG}$. Likewise, when $q_T = q_{TF}$, α_{opt} was found to be roughly one order of magnitude larger, and N_{opt} to be roughly one order of magnitude smaller than the same values when $q_T = q_{TG}$.

These results provide helpful insight into the design of a Gegenbauer reconstruction process. Although the total number of data points we require from the expanded partial sum, when $q_T = q_{TC}$ or q_{TF}, is $M_{opt} = 2N_{opt} + 1$, the value of M_{opt} when $q_T = q_{TG}$ will still be one to five times larger than when $q_T = q_{TC}$ or q_{TF}. Subsequently, a Gegenbauer reconstruction process, when $q_T = q_{TG}$, is likely to require more memory and computational bandwidth than required when $q_T = q_{TC}$ or q_{TF}. A broader comparison between the reconstruction errors realized from different expressions of q_T can be found in [21].

8 Concluding Remarks

We have described a new strategy for choosing optimal values of parameters α and N in Gegenbauer reconstruction applications whose number of expansion terms, m, is fixed. These strategies work very well provided the polynomial weighting parameter, $\lambda = \alpha N$, is not too large. The new techniques developed in this paper are equally applicable to reduce the influence of round-off errors by keeping the parameter λ fixed and allowing m to vary with N. Alternatively, they could also be used when both λ and m are fixed and only N is allowed to vary. Techniques for choosing the Gegenbauer reconstruction parameters in these circumstances are described in [20, 21].

Furthermore, although we have described using asymptotic analysis to op-

timize Gegenbauer reconstruction parameters, we also point out that these methods could be used to optimize the parameters of newer reconstruction basis sets. Finally, the techniques described in this paper all assume the underlying function analyticity, ρ or r_0, to be known. Of course, when they are not, or are known to be unfavorable, that is, indicate complex plane poles too close to the real axis, Runge phenomenon will be inescapable. Clearly there remains the need for a method of identifying any given function's analyticity. Nevertheless, until such a method is successfully developed, the methods described in this paper can still remain a model for optimizing the parameters of mainstream reconstruction methods.

Acknowledgements

The work of the authors was partially supported by the National Science Foundation under grant NSF DMS–0510813.

References

[1] M. Abramowitz and I.S. Stegun. *Handbook of mathematical functions with formulas, graphs, and mathematical tables*. National Bureau of Standards, Washington, 1972.

[2] R. Archibald, K. Chen, A. Gelb and R. Renaut. Improving tissue segmentation of human brain MRI through pre-processing by the Gegenbauer reconstruction method. *NeuroImage*, **20**(1):489–502, 2003. (Doi:10.1016/S1053-8119(03)00260-X)

[3] R. Archibald and A. Gelb. A method to reduce the Gibbs ringing artifact in MRI scans while keeping tissue boundary integrity. *IEEE Trans. Med. Imaging*, **21**:305–319, 2002. (Doi:10.1109/TMI.2002.1000255)

[4] J. Boyd. Trouble with Gegenbauer reconstruction for defeating Gibbs' phenomenon: Runge phenomenon in the diagonal limit of Gegenbauer polynomial approximations. *J. Comput. Phys.*, **20**:433–459, 2004.

[5] C. Canuto, M.Y. Hussaini, A. Quarteroni and T.A. Zang. *Spectral Methods in Fluid Dynamics*. Springer-Verlag, New York, 1988.

[6] D. Cates. *Edge detection using Fourier data with applications*. Ph.D. Dissertation, Arizona State University, 2007.

[7] P.J. Davis and P. Rabinowitz. *Methods of numerical integration*. Academic Press, Ontario, 1984.

[8] T. Driscoll and B. Fornberg. A pade-based algorithm for overcoming the Gibbs phenomenon. *Numer. Algorithms*, **26**:77–92, 2001. (Doi:10.1023/A:1016648530648)

[9] A. Gelb. On the reduction of round-off error for the Gegenbauer reconstruction method. *J. Sci. Comput.*, **20**:433–459, 2004. (Doi:10.1023/B:JOMP.0000025933.39334.17)

[10] A. Gelb and Z. Jackiewicz. Determining analiticity for parameter optimization of the Gegenbauer reconstruction method. *SIAM J. Sci. Comput.*, **27**:1014–1031, 2005. (Doi:10.1137/040603814)

[11] A. Gelb and J. Tanner. Robust reprojection methods for the resolution of the Gibbs' phenomenon. *Appl. Comput. Harmon. Anal.*, **20**:3–25, 2006.

[12] D. Gottlieb and S.A. Orszag. *Numerical analysis of spectral methods: theory and applications*. SIAM-CBMS, Philadelphia, 1977.

[13] D. Gottlieb and C.W. Shu. On the Gibbs phenomenon IV: recovering exponential accuracy in a subinterval from a Gegenbauer partial sum of a piecewise analytic function. *Math. Comput.*, **64**:1081–1095, 1995. (Doi:10.2307/2153484)

[14] D. Gottlieb and C.W. Shu. On the Gibbs phenomenon V: recovering exponential accuracy from collocation point values of a piecewise analytic function. *Numer. Math.*, **71**:511–526, 1995. (Doi:10.1007/s002110050155)

[15] D. Gottlieb and C.W. Shu. On the Gibbs phenomenon and its resolution. *SIAM Rev.*, **39**:644–668, 1997. (Doi:10.1137/S0036144596301390)

[16] D. Gottlieb and C.W. Shu. A general theory for the resolution of the Gibbs phenomenon. *Atti dei Convegni Lincei*, **147**:39–48, 1998.

[17] D. Gottlieb, C.W. Shu, A. Solomonoff and H. Vandeven. On the Gibbs phenomenon I: recovering exponential accuracy from the Fourier partial sum of a nonperiodic analytic function. *J. Comput. Appl. Math.*, **43**:81–98, 1992. (Doi:10.1016/0377-0427(92)90260-5)

[18] J.S. Hesthaven, S. Gottlieb and D. Gottlieb. *Spectral methods for time dependent problems*. Cambridge University Press, Providence, Rhode Island, 2002.

[19] Z. Jackiewicz. Determination of optimal parameters for the Chebyshev–Gegenbauer reconstruction method. *SIAM J. Sci. Comput.*, **25**:1187–1198, 2003. (Doi:.1137/S1064827503423597)

[20] Z. Jackiewicz and R. Park. A strategy for choosing Gegenbauer reconstruction parameters for numerical stability. *Appl. Math. Comput.*, **212**:418–434, 2009. (Doi:10.1016/j.amc.2009.02.034)

[21] R. Park. *Optimal compression and numerical stability for Gegenbauer reconstructions with applications*. Ph.D. Dissertation, Arizona State University, 2009.

[22] B. Shizgal and J.H. Jung. Towards the resolution of the Gibbs phenomena. *J. Comput. Appl. Math.*, **161**:41–65, 2003. (Doi:10.1016/S0377-0427(03)00500-4)

[23] H. Vandeven. Family of spectral filters for discontinuous problems. *J. Sci. Comput.*, **6**:159–192, 1991. (Doi:10.1007/BF01062118)